European Review for Medical and Pharmacological Sciences 2018; 22: 7087-7104

Osteoinductive effects of tantalum and titanium on bone mesenchymal stromal cells and bone formation in ovariectomized rats

M.-M. LU[1,2], P.-S. WU[3], X.-J. GUO[1], L.-L. YIN[1], H.-L. CAO[3], D. ZOU[1]

[1]Department of Stomatology, Shanghai Jiao Tong University Affiliated Sixth People's Hospital, Shanghai, China
[2]Department of Oral Surgery, Shanghai Stomatological Hospital, Shanghai, China
[3]State Key Laboratory of High Performance Ceramics and Superfine Microstructure, Shanghai Institute of Ceramics, Chinese Academy of Sciences, Shanghai, China

Mengmeng Lu and *Peishi Wu* contributed equally to this article

Abstract. – OBJECTIVE: Although Tantalum (Ta) exhibits better osteoinductivity in healthy subjects when compared with titanium (Ti), the relative effects in osteoporosis remain unknown.

MATERIALS AND METHODS: In this study, bone mesenchymal stromal cells of ovariectomized rats (OVX-rBMSCs) were seeded on Ta and Ti substrates for *in vitro* evaluation of cell viability, reactive oxygen species (ROS) production, alkaline phosphatase (ALP) activity, extracellular mineralization osteogenic gene and protein expression involved in bone morphogenetic protein (BMP2)/small mothers against decapentaplegic homologs 1 (Smad1) pathway. For in vivo assessment, Ta and Ti implants were embedded in femur defects of ovariectomized rats, followed by sequential fluorochrome labeling and histological staining.

RESULTS: Compared to Ti, the Ta substrates demonstrated higher viable cell percentages (96.5 ± 0.26 *vs*. 88.17 ± 2.23%), lower ROS levels (65% *vs*. Ti), and enhanced ALP activity and extracellular matrix calcification. Reverse Transcription-Polymerase Chain Reaction and Western blot assays validated the better osteoinductive effect of Ta regarding small mothers against decapentaplegic homologs 1 (Smad1), runt-related transcription factor 2, bone morphogenetic protein (BMP2), and ALP expression at both the mRNA (1.5-2-fold) and protein (1.2-1.8-fold) levels. BMP2/Smad1 signaling over-expression or knockdown yielded significantly enhanced or deteriorated OVX-rBMSC osteogenesis on the two surfaces. In addition, the Ta group revealed more new bone formation (1.3-1.5-fold *vs*. Ti) and slightly better bone-implant contact (31.82 ± 4.07 *vs*. 25.2-3.84% at 8 weeks post-implantation, $p = 0.052$) without the contribution of specific surface structures.

CONCLUSIONS: In comparison to Ti, Ta reveals better biocompatibility and osteoinductivity to OVX-rBMSCs, and the preferential Ta osteoinductivity may reflect its greater potential to trigger the BMP2/Smad1 cascade. Thus," in front of "Ta". Ta appears preferable to Ti as a bone-implant surface material under osteoporosis conditions.

Key Words:
Tantalum, Titanium, Osteoporosis, Osteogenesis, Bone morphogenetic protein 2.

Introduction

Titanium (Ti) constitutes one of the most popular biomaterials applied in bone prosthetic devices owing to its ideal biocompatibility and physiochemical properties, whereas it exerts weak osteoinductive effect[1,2]. In patients treated with Ti-based orthopedic and dental implants, osteoporosis, one of the most common bone metabolic diseases, can extend the healing period and increase the risk of undesirable osseointegration and deteriorated initial implant stability consequent to the decreased regeneration and healing potential of natural bone[3-8].

Tantalum (Ta), which boasts similar advantages to Ti, has been recently regarded as a promising alternative material for bone implants[9,10]. Moreover, numerous researches[11-15] based on healthy subjects have revealed that the osteoinductive performance of Ta is superior to that of Ti when used as bulk prostheses, implant coatings, and

Corresponding Author: Derong Zou, Ph.D; e-mail: drzou@sjtu.edu.cn
Huiliang Cao, Ph.D; e-mail: hlc@mail.sic.ac.cn

bone tissue scaffolds. However, few studies address whether Ta retains similar advantage over Ti with regard to the formation of bone from cells of subjects with osteoporosis or under osteoporotic conditions. Although Sagomonyants et al[13] reported that mineralization was significantly greater on porous Ta in comparison to that on Ti fiber mesh for osteoblasts from a high-risk osteoporosis cohort (female patients >60 years old), the diverse structures and surface morphologies of the two substrates may have masked an actual difference with regard to the intrinsic osteoinductive effect of the two biometals[16-18]. In particular, the performance of a bone prosthetic device toward improving osteogenesis is mainly determined by the inherent surface property of the applied material, as well as the structure and surface topography of the device[19,20]. As bulk substrates with a highly smooth surface may eliminate the influences of specific structures (e.g., scaffolds) and surface morphologies (e.g., nano- and porous-structured surface) on bone formation[21-23], samples of this kind should be utilized to clarify the specific osteoinductive behaviors associated with the intrinsic properties of Ta and Ti in osteoporosis.

From a biological perspective, bone mesenchymal stromal cells (BMSCs) serve as pivotal repair cells during the reconstruction of bone defect[24,25], with the preferential osteoblastic differentiation of BMSCs at the implant surface being crucial for desirable implant-bone integration[26-28]. As scholars[29-31] have affirmed the reduced osteogenic potential of BMSCs from subjects with osteoporosis, the application of implant materials with stronger osteoinductive effects on such malfunctioning cells might improve the performance of implants in osteoporosis. Also, as a crucial bone formation signal, bone morphogenetic protein 2 (BMP2) participates to a large extent in the induction of BMSC osteogenesis by regulating several signaling pathways[32,33]. Furthermore, BMP2 signaling has been demonstrated to be mediated by the activation of small mothers against decapentaplegic homologs (Smads) 1, 5, and 8 upon ligand binding[32,34]. Considering that weakened expression of the BMP2/Smads pathway is observed during the osteogenesis of osteoporotic BMSCs[35], an enhanced stimulating effect of a biomaterial on the BMP2/Smads cascade may promote the osteogenic activity of the cells.

To characterize the relative intrinsic osteoinductivity of Ta and Ti, in this work, solid Ta and Ti substrates were polished to a mirror finish to minimize the influence of surface morphology on cell behaviors[18,36,37]. BMSCs derived from ovariectomized rats (OVX-rBMSCs), the standard cell model mimicking the conditions in osteoporosis[38], were applied to systematically test the biocompatibility and intrinsic osteoinductivity of the two materials. In addition, the biological mechanism involved in the osteoinductive performance of Ta and Ti was studied by evaluating the expression of the BMP2/Smad1 signaling pathway. Finally, a femur defect model in ovariectomized rats was used to investigate the influence of Ta and Ti samples on bone formation *in vivo*.

Materials and Methods

Sample Preparation

Pure Ta and Ti sheets with a thickness of 0.5 mm were incised into samples with different dimensions, including square substrates (10×10 mm and 20×20 mm) for *in vitro* studies and rectangular implants (5×3 mm) for *in vivo* animal experiments. One side of each sample was polished to a mirror finish for evaluation. All samples were sterilized with 75% alcohol for 3h and washed twice with sterile phosphate-buffered saline (PBS) prior to use.

Characterization of the Material Surface

The surfaces of the Ta and Ti samples with similar roughness (42.87 ± 2.35 nm for Ta and 42.95 ± 5.13 nm for Ti) were featureless at the nanoscale and spontaneously oxidized during exposure to the atmosphere. Furthermore, the amounts of Ta and Ti ions released by corresponding samples were all below the detectable limit of inductively-coupled plasma optical emission spectrometry (Vista AX, Varian, Palo Alto, CA, USA) (< 0.002 μg/ml for Ti, < 0.01 μg/ml for Ta).

In Vitro Studies

Osteoporotic Rat Model Preparation

Healthy female Sprague-Dawley rats (3-month-old) were used in this investigation. The experimental protocols were approved by the Animal Care and Use Committee of Sixth People's Hospital Affiliated to Shanghai Jiaotong University. Ovariectomy was carried out to establish osteoporotic rat models as previously described[39]. Briefly, chloral hydrate (350 mg/kg) was injected

into the abdominal cavity for anesthesia. After two longitudinal incisions were made along both sides of the spine, the ovarian vessels and fallopian tubes were ligated and the bilateral ovaries were excised. Sham-operated rats, in which only fat around the ovaries was removed, were used for osteoporotic model verification using micro-computed tomography analysis 3 months after the surgery.

Cell Isolation and Culture

After model validation, OVX-rBMSCs were obtained and cultured as previously described[39]. The primary cells were cultured in complete medium [CM; Dulbecco's Modified Eagle Medium (Gibco, Grand Island, NY, USA) with 10% fetal bovine serum (Gibco), 100 U/ml penicillin and 100 μg/ml streptomycin] at 37°C in a 5% CO_2 incubator. Adherent cells were subcultured using trypsin/ethylenediaminetetraacetic acid (EDTA, Sigma-Aldrich, St. Louis, MO, USA) (0.25% w/v trypsin, 0.02% EDTA) when 80-90% confluence was reached. To evaluate the effects of the Ta and Ti samples on cell behavior (using cells at passage 3-5), culture plastic (Cp) with the same size and shape were applied as a control.

Initial Cell Adherent Number Assay

The OVX-rBMSCs (1.5×10^4 cells/well) were seeded on the substrates (10×10 mm) in 24-well plates and cultured in complete medium (CM). At 1, 6, and 24h, the adherent cells were fixed in 4% formaldehyde solution for 10 min and stained with 4′,6-diamidino-2-phenylindole (DAPI) for 5 min (Beyotime, Shanghai, China). The cell numbers were counted in 10 random fields on substrates of each type under a fluorescence microscope (IX 70, Olympus, Tokyo, Japan).

Cell Proliferation Assay

The OVX-rBMSCs (1×10^4 cells/well) were seeded on different substrates (10×10mm) in 24-well plates. After culturing in CM for 1, 3, 5, and 7 days, cell proliferation was assessed using the CCK-8 assay (Dojindo, Kumamoto, Japan). At each time point, the substrates were washed with PBS and transferred to new 24-well plates. Then, 1 ml mixed solution (a-MEM medium and CCK-8 solution with a ratio of 10:1) was added to each well and incubated at 37°C for 4h. After incubation, 100 μl of the suspension was introduced to a 96-well plate and the absorbance was read at 450 nm.

Cell Viability Assay

The OVX-rBMSCs (2×10^6 cells/well) were inoculated on the substrates (20×20 mm) in 6-well plates and cultured in CM. On day 1 and 3, the substrates were transferred to new plates and the cells were trypsinized and washed with PBS. The cells were resuspended in 1 ml PBS and cell counting was conducted. Next, 1×10^6 cells from each substrate were stained with Annexin V-Fluorescein isothiocyanate (FITC) (Beyotime) for 15 min and propidium iodide (PI; Beyotime) in the dark for 5min. The fluorescence of individual cells was measured using flow cytometry (FCM; Accuri C6, Becton Dickson, Bedford, MA, USA).

Detection of Reactive Oxygen Species (ROS) Production

The OVX-rBMSCs (2×10^6 cells/well) were seeded on substrates (20×20 mm) in 6-well plates and cultured in CM for 1 and 3 days, then digested and washed with PBS. Next, 1×10^6 cells from each substrate were incubated with 2′,7′-dichlorofluorescein diacetate (DCFH-DA; Beyotime) in the dark for 30 min. The fluorescence intensity was analyzed by FCM (Accuri C6).

Alkaline Phosphatase (ALP) Activity Assay

To evaluate the osteoinductive effects of Ta and Ti, OVX-rBMSCs (1×10^4 cells/well) were added on the substrates (10×10 mm) in 24-well plates and cultured in osteogenic medium [OM; CM supplemented with 50 M ascorbic acid (Sigma-Aldrich, St. Louis, MO, USA), 10 mM b-glycerophosphate (Sigma-Aldrich), and 100 nM dexamethasone (Sigma-Aldrich)] or CM. On day 7 and 14, the ALP activity was measured using an ALP activity assay kit (Nanjing Jiancheng Bioengineering Institute, Nanjing, China). The substrates were washed with cold PBS and transferred to new plates. The attached cells were lysed by lysis buffer RIPA; (Beyotime) on ice. After the lysates reacted with a working solution at 37°C for 15 min, the optical density (OD) values of the resulting solutions were determined at a wavelength of 520 nm. The ALP levels were normalized to the total intracellular protein content using the bicinchoninic acid (BCA) protein kit (Beyotime).

ALP staining was also performed using a BCIP/NBT ALP color development kit (Beyotime) on day 7. Briefly, substrates were fixed in 4% formaldehyde solution for 10 min, then the BCIP/NBT working solution was added to each well and incubated in the dark for 30 min. Subsequently, the substrates were rinsed with distilled water and observed using a microscope (IX 70).

Extracellular Matrix (ECM) Mineralization Assay

To identify the results of OVX-rBMSC osteogenesis on the substrates, ECM mineralization was evaluated. Cells (5×10^3 cells/well) were seeded on samples (10×10 mm) in 24-well plates and cultured in OM. On day 14 and 21, the substrates were washed with PBS and transferred to new plates, fixed in 0.5 ml 75% ethanol for 1h, and stained with 40 mM Alizarin red S (ARS; Solarbio, Beijing, China) for 10 min. The unbound red residue was rinsed with PBS and images were obtained using optical microscopy (IX 70). Subsequently, the bound stain was eluted using 10% cetylpyridinium chloride (Sigma-Aldrich, St. Louis, MO, USA) in 10 mM sodium phosphate, and the OD values were measured at 600 nm.

Osteogenic Gene Expression Assay

The OVX-rBMSCs were seeded on different substrates (20×20 mm) in 6 well plates and cultured in OM and CM. The cell density was 5×10^5 cells/well (cultured for 1 day), 1×10^5 cells/well (for 7 days), and 5×10^4 cells/well (for 14 days). At each time point, the mRNA expression of Smad1, runt-related transcription factor 2 (RUNX2), BMP2, ALP, osteoprotegerin (OPG), and receptor activator for nuclear factor-κ B ligand (RANKL) was measured by Real-Time Reverse Transcriptase-Polymerase Chain Reaction (RT-PCR). The substrates were washed with PBS and transferred to new wells, and the RNA was extracted using TRIzol reagent (Invitrogen, Carlsbad, CA, USA). An equivalent amount of RNA from each sample was reverse transcribed into cDNA using the PrimeScript RT reagent Kit (TaKaRa, Otsu, Shiga, Japan) according to the manufacturer's protocol. Then, RT-PCR analysis was performed on the Bio-Rad C1000 using SYBR Premix Ex Taq (TaKaRa). The expression level of the housekeeping gene *Gapdh* was used to normalize that of the target genes. The primers for the target genes are listed in Table I.

Osteogenic Protein Expression Assay

The OVX-rBMSCs were seeded on different substrates (20×20 mm) in 6-well plates and cultured in OM and CM. The cell density was 5×10^5 cells/well (cultured for 1 day), 1×10^5 cells/well (for 7 days), and 5×10^4 cells/well (for 14 days). At each time point, the protein expression of RUNX2, BMP2, ALP, phosphorylated Smad1 (p-Smad1), and total Smad1 (T-Smad1) was measured by Western blot. Total protein extraction was carried out with RIPA lysis buffer followed by centrifugation at 12,000×*g* at 4°C for 20 min, then proteins in cell lysates were separated by 10% sodium dodecyl sulfate-polyacrylamide gel electrophoresis and transferred to a polyvinylidene difluoride membrane (Bio-Rad, Hercules, CA, USA). Blots were blocked using skim milk for 1h and then incubated with primary antibodies against p-Smad1 (1:500; Abcam, Cambridge, MA, USA), Smad1 (1:800; Abcam), BMP2 (1:500; Abcam), RUNX-2 (1:1000; Abcam), ALP (1:3000; PLLabs, Vancouver, Canada) or GAPDH (1:2000; Cell Signaling Technology, Danvers, MA, USA) at 4°C overnight. Subsequently, peroxidase-conjugated secondary antibodies (1:1000; Beyotime) were further used for 2h at room temperature. Blots were analyzed using an enhanced chemiluminescence (ECL) detection kit (Pierce, Rockford, IL, USA).

Table I. Primers for the target genes.

Gene	Sequence	Size (bp)
Smad1-forward	5′-GTGGAAACAGGGCGACGAAG-3′	156
Smad1-reverse	5′-AGGGAGCGAGGAATGGTGAC-3′	
RUNX2-forward	5′-ACTTCGTCAGCGTCCTATC-3′	148
RUNX2-reverse	5′-CATCAGCGTCAACACCATC-3′	
BMP2-forward	5′-ACGACGGTAAAGGACATC-3′	221
BMP2-reverse	5′-ATGGTTGGTGGAGTTCAG-3′	
ALP-forward	5′-AAGCACTCCCACTATGTC-3′	125
ALP-reverse	5′-GTCAGGTTGTTCCGATTC-3′	
OPG-forward	5′-CTGGGCTGTTTCTTCAGGATG-3′	224
OPG-reverse	5′-CTCTTTCTCAGGGTGCTTGAC-3′	
RANKL-forward	5′-CATCAGCGTCAACACCATC-3′	228
RANKL-reverse	5′-TTTATGGGAACCCGATGGGATG-3′	
GAPDH-forward	5′-GTCGGTGTGAACGGATTTG-3′	181
GAPDH-reverse	5′-TCCCATTCTCAGCCTTGAC-3′	

Cell Transfection and Inhibitor Application

The specific BMP2 coding sequence (BMP2-CDS, Sangon Biotech Co., Ltd., Shanghai, China) was cloned into the pCDNA3.1 (+) vector (Addgene, Cambridge, MA, USA). The primers were as follow: BMP2-CDS-forward: CCCAAGCTTATGGTGGCCGGGACCCGCTGT (5′–3′), BMP2-CDS-reverse: CCGGAATTCGCGACACCCGCAACCCTCCAC (5′–3′). For the overexpression of BMP2, the OVX-rBMSCs (3×10^5cells/well) were transduced with pCDNA3.1 (+)-BMP2-CDS and incubated for 6 h. The cells treated with blank pCDNA3.1 (+) vector were used as a negative control (NC). Alternatively, the cells (3×10^5 cells/well) were transfected with 0.1μM Smad1-siRNA and also incubated for 6h to knock down Smad1 expression. The sequences were as follow: Smad1-siRNA1, nt (685–707), AGGAAGUCUGCAUCAAUCCTT (5′–3′); Smad1-siRNA2, nt (1288–1310), AUGUUAACCGGAACUCCACTT (5′–3′); Smad1-siRNA3, nt (1767–1789), and ACUAUUGGGCCUUGCAUGUTT (5′–3′). The cells treated with scrambled siRNA were applied as NC. The cell transfection was conducted using Lipofectamine reagent (Invitrogen, Carlsbad, CA, USA) according to the manufacturer instruction. Serum-free medium was applied in all the transfection processes, and the transfection efficiency was determined using RT-PCR and Western blot assays.

The OVX-rBMSCs with down-regulated Smad1 expression were seeded on the Ta substrates (20×20 mm) in 6-well plates and cultured in CM. Additionally, cells without transfection on the Ta substrates were treated with 100 nM BMP2 inhibitor (LDN-193189) (Selleck, Shanghai, China) for 24h after cell seeding. In addition, the OVX-rBMSCs with BMP2 overexpression, followed with or without Smad-1 knockdown, were incubated on the Ti substrates. The cell seeding density was 5×10^5 cells/well for 1 day of culture and 1×10^5 cells/well for 7 days. On day 1 and 7, the expression of p-Smad1, T-smad1, RUNX2, ALP, and BMP2 was examined by RT-PCR and Western blot assays. The ALP activity was also measured.

In Vivo Studies

Surgical Procedure

The surgical procedures were conducted under sterile conditions. The OVX-rats were anesthetized by intraperitoneal injection of ketamine (10 mg/kg). Each rat was immobilized with the knee joint in maximally flexed position and both thighs were shaved and depilated, and the surgical sites were sterilized with iodophor disinfectant. One bone defect (5×3×0.5 mm) parallel to the long axis of each femur was made on the shaft using piezosurgery (Mectron, Carasco, Italy) with a 5×3×0.5 mm; OT7 working tip (Figure 6A) until exposure of the marrow. The bone defects were washed with physiological saline and the implants were pressed into the prepared defects (Figure 6B), then the wound was closed carefully. A total of 20 OVX-rats were randomly divided into four groups corresponding to Ta (4 weeks), Ti (4 weeks), Ta (8 weeks), and Ti (8 weeks).

Sequential Fluorescent Labeling Assay

To characterize the new bone formation and mineralization, a polychrome sequential fluorescent labeling method was used. 20 and 40 days after the operation, two fluorochromes were administered intraperitoneally with a sequence of 30mg/kg ARS (Sigma-Aldrich, Saint Louis, MO, USA), and 20 mg/kg calcein (Sigma-Aldrich).

Sample Preparation and Hstological Evaluation

The OVX-rats were sacrificed 8 weeks after the operation. The femurs inserted with the implants were harvested and fixed in 10% buffered formaldehyde for histomorphometric observation. Femur specimens were dehydrated in ascending concentrations of ethanol (70, 80, 90, 95, and 100 v/v%), and embedded in polymethylmethacrylate. The embedded specimens were cut into 150-μm-thick sections perpendicular to the long axis of the bone using a Leica SP1600 saw microtome (Leica, Wetzlar, Germany) and processed to a final thickness of approximately 80μm. The polished surface of each implant was observed. The fluorescence labeling analysis for mineralized bone tissue was conducted using a confocal laser scanning microscope (Leica SP8, Wetzlar, Germany), and the excitation/emission wavelengths to observe chelating fluorochromes were 543/620 nm and 488/520 nm for ARS (red) and calcein (green), respectively. After fluorescence microscopy, the sections were counter-stained with Van Gieson's picrofuchsin and methylene blue, and measured for bone-implant contact (BIC) rate. The images were captured with a microscope (IX 70) and analyzed using Image-Pro Plus 6.0 software (Media Cybernetics Inc., Rockville, MD, USA).

Statistical Analysis

All data are expressed as the means ± standard deviation. Statistical analysis was conducted by one-way ANOVA analysis following Dunnett post-hoc test and two-way ANOVA analysis following Bonferroni post-hoc test for *in vitro* studies (n=3) and Student's *t*-test for *in vivo* studies (n=5) using SPSS 22 software (SPSS Inc., Chicago, IL, USA). $p < 0.05$ was considered to indicate statistically significant differences.

Results

Osteoporotic Model Verification

As shown in Figure S1B, the ovariectomized rats revealed a 40% decrease with regard to the bone mineral density (BMD) of the cancellous bone in comparison to the sham-operated ones (0.099 ± 0.015 and 0.058 ± 0.013 g/cm^2, respectively). This result indicated the successful establishment of the osteoporotic rat model[40].

In vitro studies

Initial Adhesion of OVX-rBMSCs on Substrates

Quantitative analysis of cell adhesion on different substrates was conducted by DAPI staining (Figure 1A). The results showed that the cell numbers on the Ta, Ti, and Cp substrates were 48 ± 10, 42 ± 9, and 54 ± 9 at 1h, 74 ± 16, 70 ± 21, and 78 ± 17 at 6h, 163 ± 15, 168 ± 20, and 174 ± 26 at 24h. The cell quantities on the Ta and Ti substrates were significantly less at 1h in comparison to those on Cp. However, such a difference could not be observed at 6 and 24h (Figure 1B).

OVX-rBMSC Proliferation on Substrates

Cell proliferation was measured using the CCK-8 assay. On day 1 and 3, the OVX-rBMSC numbers on the three substrates were similar at each time point. After culturing for 5 and 7 days, cell proliferation on the Cp substrate was significantly faster than that on Ta and Ti substrates, with no significant difference between the Ta and Ti substrates (Figure 1C).

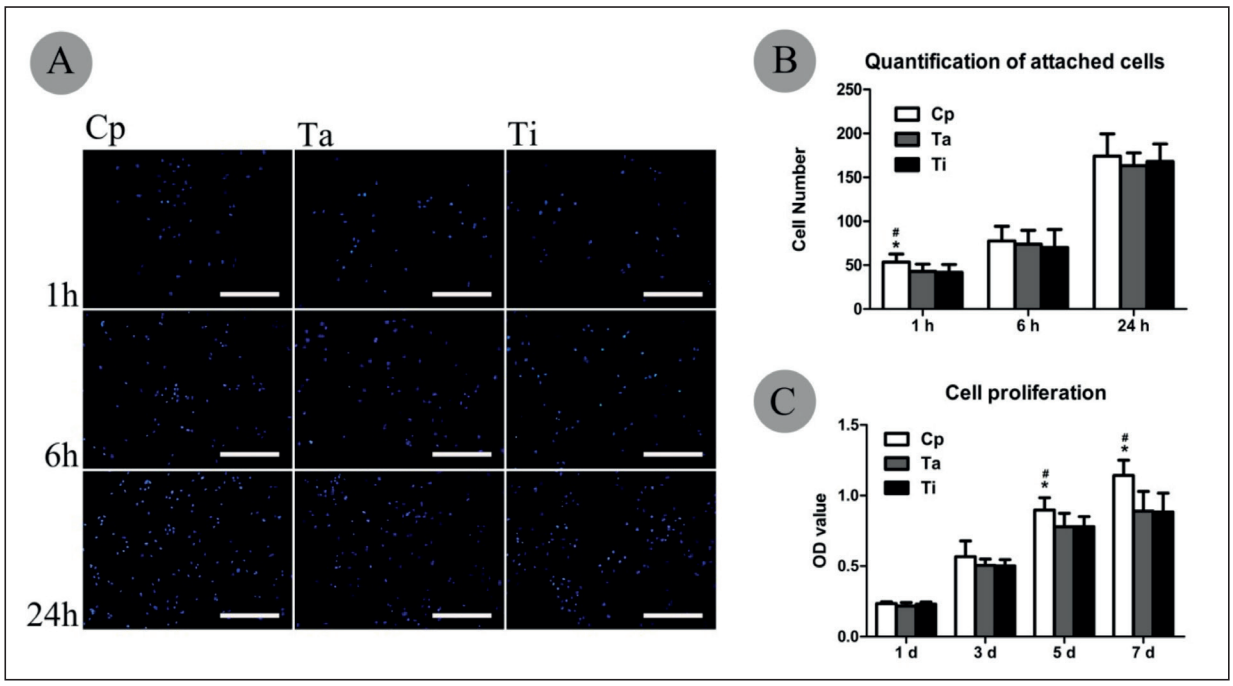

Figure 1. Initial adhesion and proliferation of OVX-rBMSCs on Ta, Ti, and Cp substrates. ***A,*** Initially attached cells on three substrates stained by DAPI at 1, 6, and 24h; scale bar represents 500 μm; ***B,*** quantification of adherent cells at the corresponding time points; and ***C,*** cell proliferation measured by CCK8 at 1, 7, and 14 days. The comparison was conducted among substrates at the same time points. $^{\#}p < 0.05$ compared with Ta, $^{*}p < 0.05$ compared with Ti.

Viability and ROS production of OVX-rBMSCs on substrates

The viability of OVX-rBMSCs on different substrates was monitored by Annexin V-FITC staining with FCM. On day 1 and 3, the highest number of normal cells was identified on the Cp substrates. In addition, more viable cells were observed on the Ta substrate in comparison to those on the Ti substrate (96.37 ± 0.56% *vs.* 93.33 ± 0.49% on day 1; 96.5 ± 0.26% *vs.* 88.17 ± 2.23% on day 3, respectively) (Figure 2A, B).

The intracellular ROS level in OVX-rBMSCs was determined by evaluating the intensity of 2',7'-dichlorofluorescein fluorescence. The cells on the Cp substrates revealed the lowest ROS level at each time point; moreover, the fluorescence intensity on the Ta substrate was lower than that on the Ti substrate on day 3 (6.37 ± 0.53- fold *vs.* 9.76 ± 0 .81-fold, respectively, compared to Cp) (Figure 2C, D).

ALP activity of OVX-rBMSCs on Ta and Ti substrates

In OM and CM, the cells on the Ta surface showed higher ALP activity (19.24 ± 1.57 and 27.32 ± 2.58 King unit/g prot in OM on day 7 and 14; 9.88 ± 0.9 and 14.06 ± 1.48 in CM on day 7 and 14, respectively) when compared with those on the Cp and Ti surfaces at the two time points. In addition, the Ti surface manifested higher ALP activity as compared to the Cp surface on day 7 in both media (Figure 3B). The results of the ALP activity assay were also verified by ALP

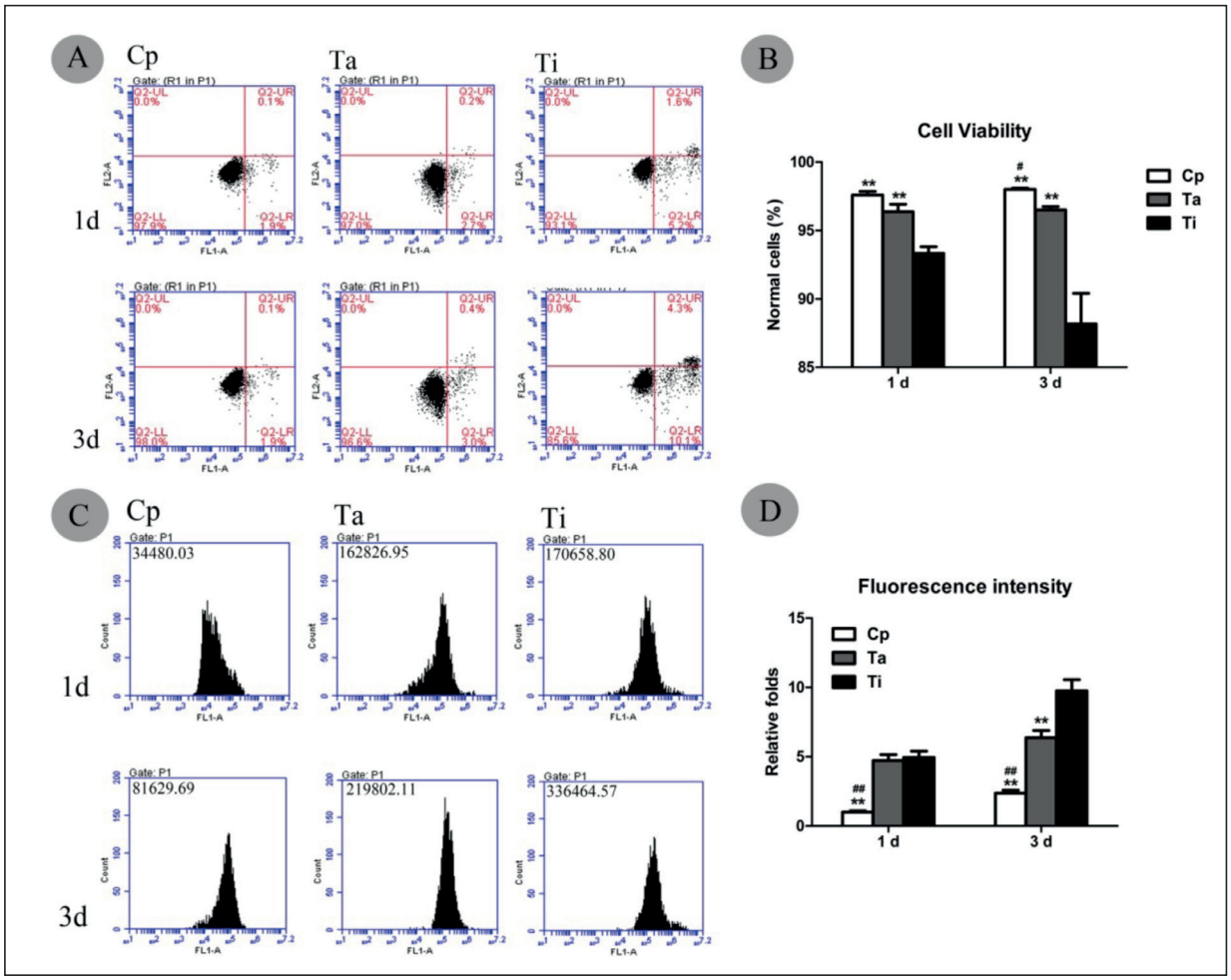

Figure 2. Biocompatibility of Ta, Ti, and Cp substrates toward OVX-rBMSCs. ***A, B,*** Percentage of viable cells on different substrates as measured by Annexin V-FITC and FCM at day 1 and 3; ***C, D,*** fluorescence intensity of ROS production on different substrates measured by DCFH-DA and FCM at day 1 and 3; the ROS level of Cp at day 1 was used for normalization. The comparison was conducted among substrates at the same time points. $^{\#}p < 0.05$, $^{\#\#}p < 0.01$ compared with Ta; $^{**}p < 0.01$ compared with Ti.

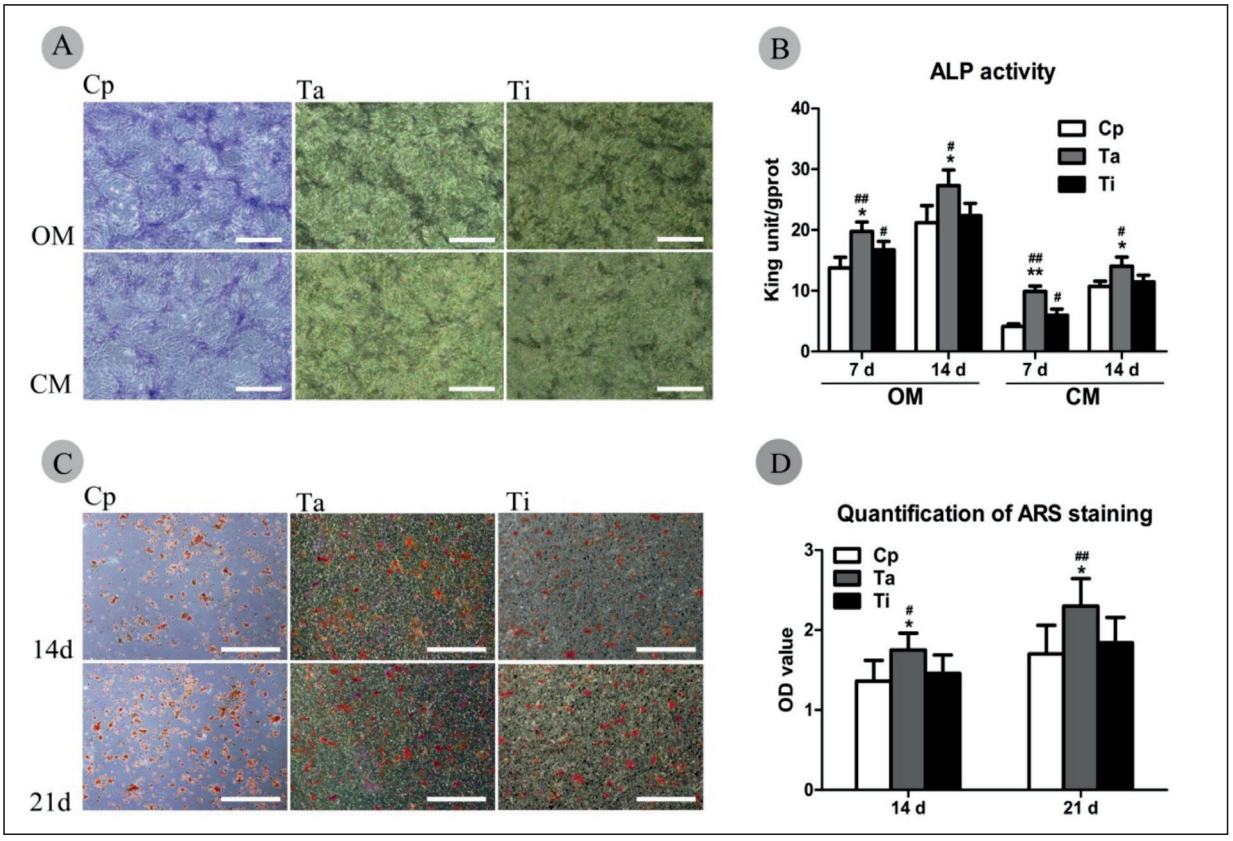

Figure 3. OVX-rBMSC osteogenesis on Ta, Ti, and Cp substrates. ***A,*** ALP staining on different substrates cultured in OM and CM for 7 days; scale bar represents 500 μm. ***B,*** ALP activity on different substrates cultured in OM and CM for 7 and 14 days. ***C,*** ARS staining on different substrates cultured in OM for 14 and 21 days; scale bar represents 1 mm; ***D,*** quantification of ARS staining at the corresponding time points. The comparison was conducted among substrates at the same time points. $^{\#}p < 0.05$, $^{\#\#}p < 0.01$ compared to Cp; $^{*}p < 0.05$, $^{**}p < 0.01$ compared to Ti.

staining on different substrates cultured in OM and CM for 7 days (Figure 3A).

ECM Mineralization on Ta and Ti Substrates

After 14 and 21 days, the cells were stained with ARS and analyzed using light microscopy images (Figure 3C). As shown by the ARS quantification results, the number of calcium nodules in ECM on the Ta substrate was higher than those on the Ti and Cp substrates at these stages (Figure 3D). However, differences between the Ti and Cp substrates at each time point were not statistically significant.

Osteogenic Gene and Protein Expression of OVX-rBMSCs on Ta and Ti Substrates

Real-time RT-PCR was used to evaluate the influence of different substrates on OVX-rBMSC osteogenesis at a molecular level. For the same substrates, OM enhanced the expression of Smad1, RUNX2, BMP2, ALP, and OPG compared with CM. As shown in Figure 4A-E, in each medium, the highest expression of the above genes was observed on the Ta substrates (approximately 1.5-2-fold *vs.* Ti); whereas the gene expression was only slightly up-regulated on the Ti substrates in comparison to that on the Cp substrates. Moreover, the lowest gene expression of RANKL was also observed on the Ta substrate (Figure 4F). Also, the influence of the three substrates on the expression of the BMP2/Smad1 pathway, down-stream effector RUNX2, and ALP was further measured by Western blotting (Figure 4G-K; Figure S2). The results demonstrated that the protein expression of BMP2, RUNX2, and ALP, as well as Smad1 phosphorylation also reached the highest level on the Ta surface (approximately 1.2-1.8-fold *vs.* Ti). In

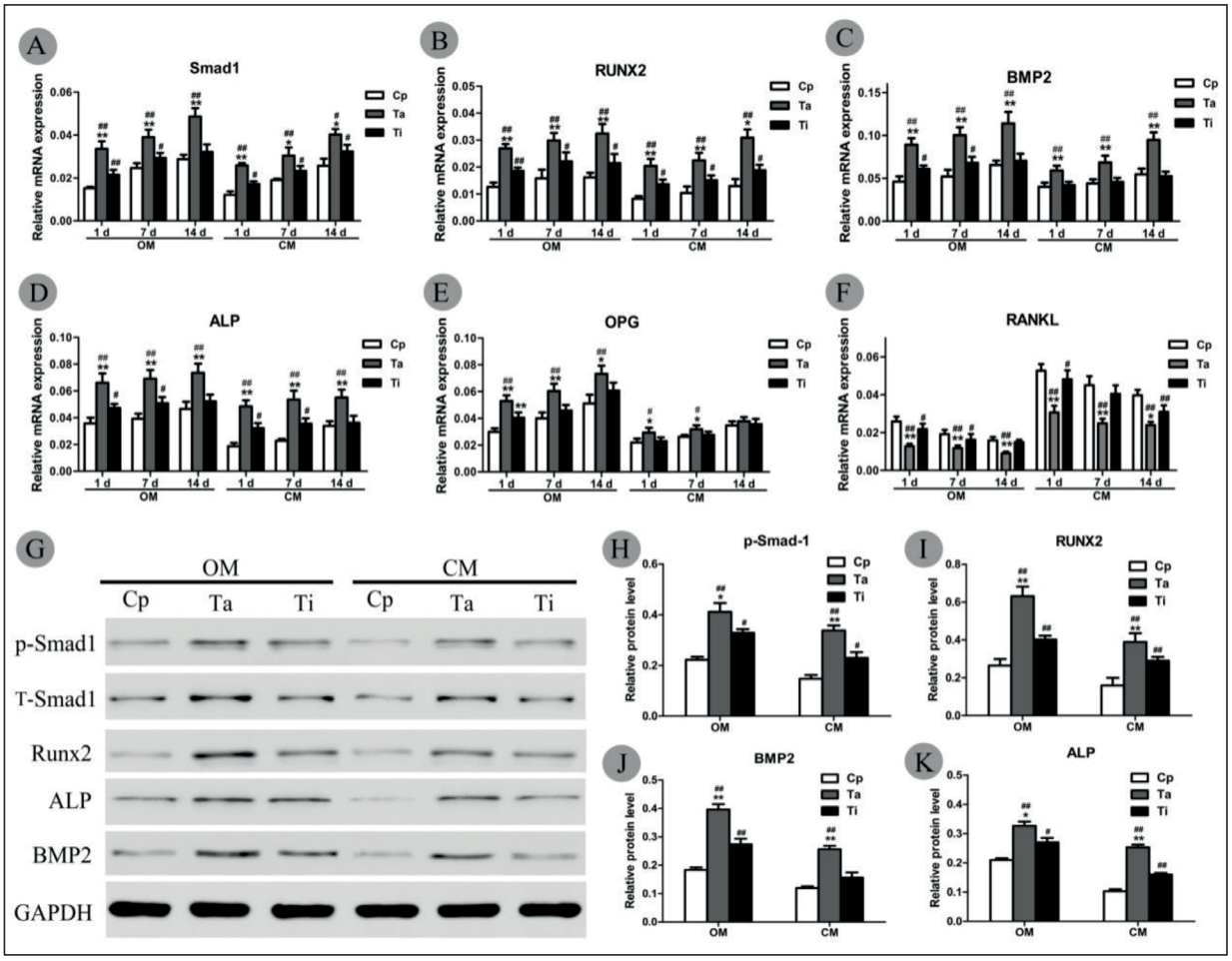

Figure 4. Osteogenesis-related gene and protein expression of OVX-rBMSCs on Ta, Ti, and Cp substrates. mRNA expression of ***A,*** Smad1, ***B,*** RUNX2, ***C,*** BMP, ***D,*** ALP, ***E,*** OPG, and ***F,*** RANKL on different substrates in OM and CM as evaluated by RT-PCR analysis at day 1, 7, and 14. The expression level of *Gapdh* was used to normalize that of the target genes. ***G,*** Protein expression of cells on different substrates in both media as detected by Western blot at day 1, and corresponding band gray values of ***H,*** p-Smad1, ***I,*** RUNX2, ***J,*** BMP2, and ***K,*** ALP. The expression level of GAPDH was used to normalize that of the target proteins. The comparison was conducted among substrates at the same time points. $^{\#}p < 0.05$, $^{\#\#}p < 0.01$ compared to Cp; $*p < 0.05$, $**p < 0.01$ compared to Ti.

general, the variation of Smad1, RUNX2, ALP, and BMP2 in OVX-rBMSCs at the protein level on different substrates was consistent with their mRNA expression.

Role of the BMP2/Smad1 Pathway in OVX-rBMSC Osteogenesis Mediated by the Ta and Ti Surface

Following transfection with Smad1-siRNA2, OVX-rBMSCs exhibited an 80% reduction of mRNA expression compared with the wild-type (control) or cells treated with scrambled siRNA (negative control, NC) (Figure S3A). The transfection efficiency was also verified by a 70% decrease at the protein level (Figure S3B, C). Owing to its higher transfection efficiency in comparison to Smad1-siRNA1 and Smad1-siRNA3, Smad1-siRNA2 was used in the following experiments. Conversely, after OVX-rBMSCs were transduced with BMP2-CDS, the mRNA expression increased by 4-fold in comparison to that in the control or NC (Figure S3D). The transfection efficiency was further confirmed by the tripled expression of BMP2 at the protein level (Figure S3E, F). However, in the above two transfection procedures, no significant difference was identified for either mRNA and protein expression between NC and control for the target genes.

On the Ta surface, the downregulation of BMP2 or Smad1 significantly suppressed the gene expression of RUNX2 and ALP in OVX-rBMSCs (a 50-70% decrease compared with that in the NC; Figure 5B, D), which was in agreement with the 30-50% reduction at the protein level (Figure 5E, G, I; Figure S4A, C, E). Moreover, the decreased expression of RUNX2 and ALP on the Ta surface reached a similar level when compared with that in the NC on the Ti surface. In addition, the knockdown of BMP2 expression diminished the expression of Smad1 and vice versa (Figure 5A, C, E, F, H; Figure S4A, B, D).

On the Ti surface, the upregulation of BMP2 markedly elevated the expression of RUNX2 and ALP (approximately a 2-fold and 0.5-1-fold

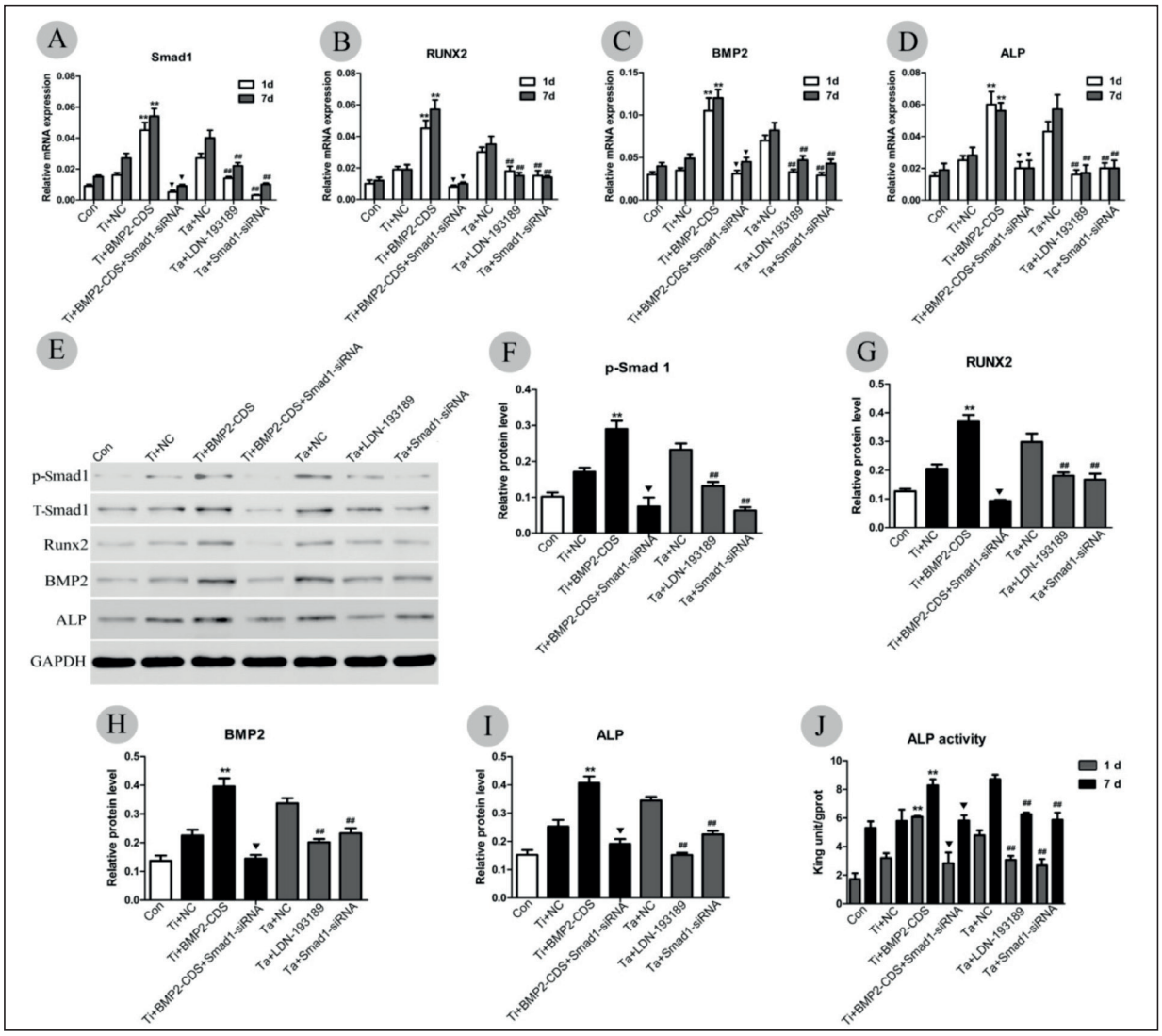

Figure 5. Role of BMP2/Smad1 signaling in OVX-rBMSC osteogenesis on Ta and Ti substrates. mRNA expression of ***A,*** Smad1, ***B,*** RUNX2, ***C,*** BMP2, and ***D,*** ALP in cells treated with blank pCDNA3.1(+)vector (negative control, NC), pCDNA3.1(+)-BMP2 (BMP2-CDS), or BMP2-CDS with Smad1-siRNA (BMP2-CDS+Smad1-siRNA) on Ti substrates and those transfected with scramble siRNA (NC), BMP2 inhibitor (LDN-193189), or Smad1-siRNA on Ta substrate in CM detected by RT-PCR at day 1 and 7. The expression level of *Gapdh* was used to normalize that of the target genes. ***E,*** Protein expression of cells on different substrates as detected by Western blot at 1 day after transfection, and corresponding band gray values of ***F,*** p-Smad1, ***G,*** RUNX2, ***H,*** BMP2, and ***I,*** ALP. The expression level of GAPDH was used to normalize that of the target proteins and the corresponding expression of wild-type OVX-rBMSCs on Cp substrates was used as a blank control (con). ***J,*** ALP activity of OVX-rBMSCs on different substrates at 1 and 7 days after transfection. $^{\#\#}p < 0.01$ compared with NC on Ta substrates at the same time point; $^{**}p < 0.01$ compared to NC, $^{\blacktriangledown}p < 0.01$ compared to BMP2-CDS on Ti substrates at the same time point.

increase at the mRNA and protein level, respectively) as well as Smad1 phosphorylation (Figure 5B, D, E-G, I; Figure S4A). Moreover, a similar level of increase was observed in comparison to that in the NC on the Ta surface. In addition, the subsequent Smad1 inhibition abrogated the enhanced expression of RUNX2 and ALP induced by the over-expression of BMP2 (Figure 5B, D, E, G, I; Figure S4A, C, E).

Finally, the variation of OVX-rBMSC osteogenesis on the Ta and Ti substrates caused by the up- and down-regulation of the BMP2/Smad1 pathway was concordant to the alteration of ALP activity at the corresponding time points (Figure 5J).

In Vivo Studies

Bone-Implant Contact (BIC) of Ta and Ti Implants

The histological sections were stained with van Gieson's picrofuchsin and methylene blue. From the transverse point of view, newly formed bone attached and extended on the part of the Ta and Ti surface, whereas gaps infiltrated by fibrous tissues were also observed between the implant surface and the bone tissues in both groups. The Ta group displayed a slightly higher percentage of BIC in comparison to the Ti group (31.82 ± 4.07% *vs.* 25.2 ± 3.84%) at 8 weeks after implantation ($p = 0.052$; Figure 6D, E).

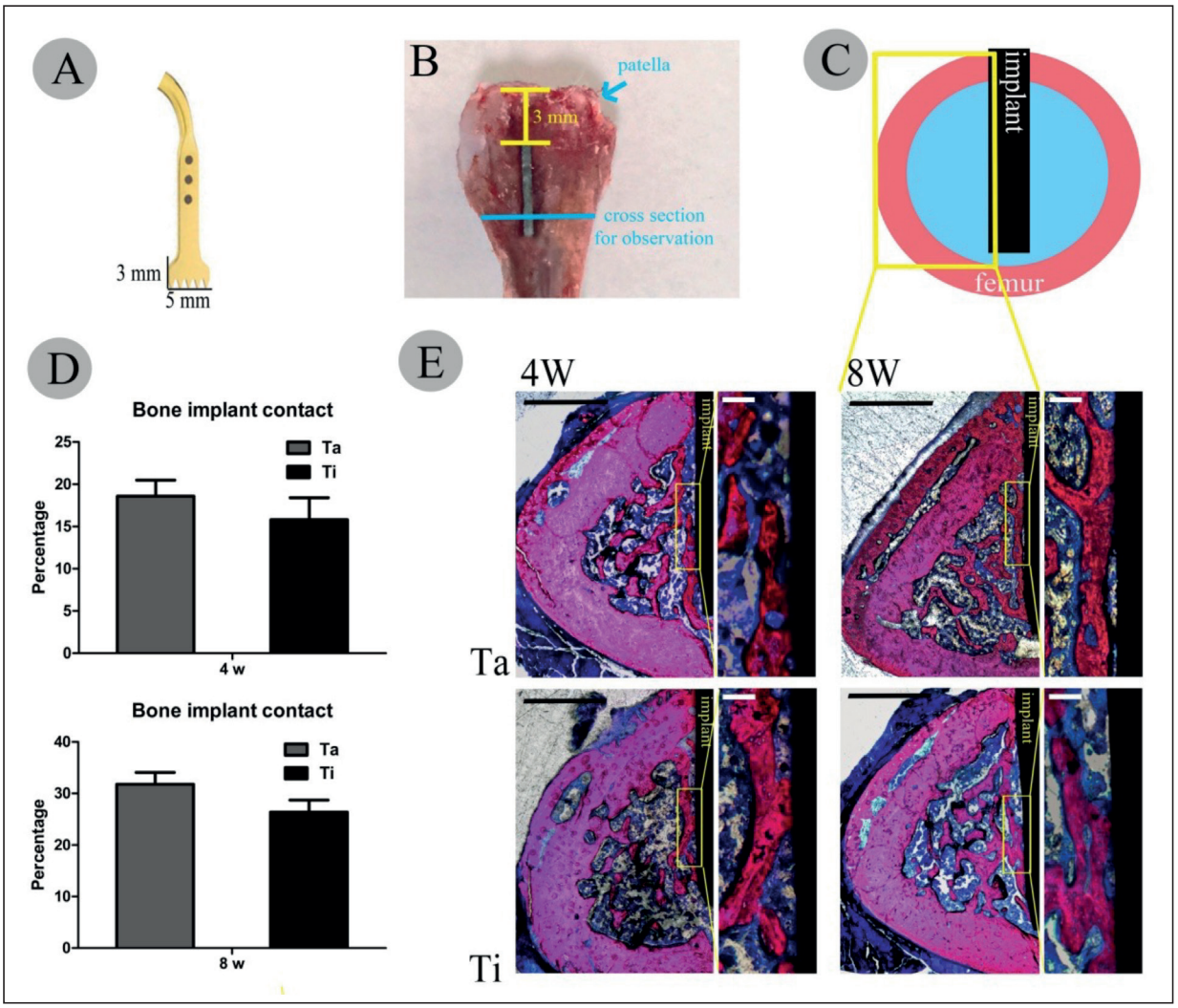

Figure 6. Histological analysis of osseointegration of Ta and Ti implants in ovariectomized rats. ***A,*** Working tip used in operation; ***B,*** position of implant in the femur; ***C,*** region of histological section for observation; ***D,*** bone-implant contact (BIC) rate at 4 and 8 weeks after implantation, and ***E,*** relevant Van Gieson's picrofuchsin and methylene blue staining of histological sections. Red and blue stain indicates bone and soft tissue, respectively; black scale bar represents 1mm, white scale bar represents 100 μm.

Bone Formation on the Surface of Ta and Ti Implants

Fluorochrome labeling was conducted to assess the new bone formation and mineralization on the polished surface of Ta and Ti implants at time intervals of 20 and 40 days. More calcein was incorporated into the bone along the Ta implant surface (Figure 7A). In addition, the percentage of ARS- and the calcein-labeled area in the Ta group was approximately 1.5- and 1.3-fold that in the Ti group, respectively (Figure 7B).

Discussion

To reduce the risk of implant failure in osteoporosis, numerous surface modification methods, such as increasing surface roughness, producing nano- and porous-structure, as well as fabricating osteoinductive coating, have been utilized to enhance the bone forming potency of implant materials[41-44]. Nevertheless, the intrinsic osteoinductivity of the materials still plays a crucial role in successful implant osseointegration[45,46]. Therefore, unlike other research reports, the present study employed Ta and Ti samples with a highly polished surface to eliminate the effects of surface processing and investigate the performance determined by the inherent property of the two materials under osteoporotic conditions. As both Ta and Ti samples featured similar unstructured surfaces with nano-scale roughness, we believe that the surface morphology did not facilitate osteogenesis *in vitro* or *in vivo*[22,23,47]. Moreover, considering the low degree of ion release from either Ta or Ti, we consider that the different oxide layers overlaying the two sample surfaces served as the major factor underlying the different cell behaviors and osteogenesis of these samples *in vitro* and *in vivo*.

In general, the attachment numbers (Figure 1B) on the Ta and Ti substrates were similar to those on the Cp substrates during the first 24h, denoting the ideal property of Ta and Ti toward OVX-rBMSCs at the first phase of cell-material interaction. Although greater numbers of attached cells were identified on the Cp substrate at 1h, such a difference could be attributed to the better hydrophilicity of Cp[48]. Moreover, the cell viability and ROS production assays revealed the best biocompatibility of the Cp substrates toward OVX-rBMSCs[49,50], which was consistent with Cp exhibiting the fastest cell proliferation. Notably, although the Ta substrates showed a higher percentage of viable cells and a lower ROS level in comparison to the Ti substrates (Figure 2), no significant dif-

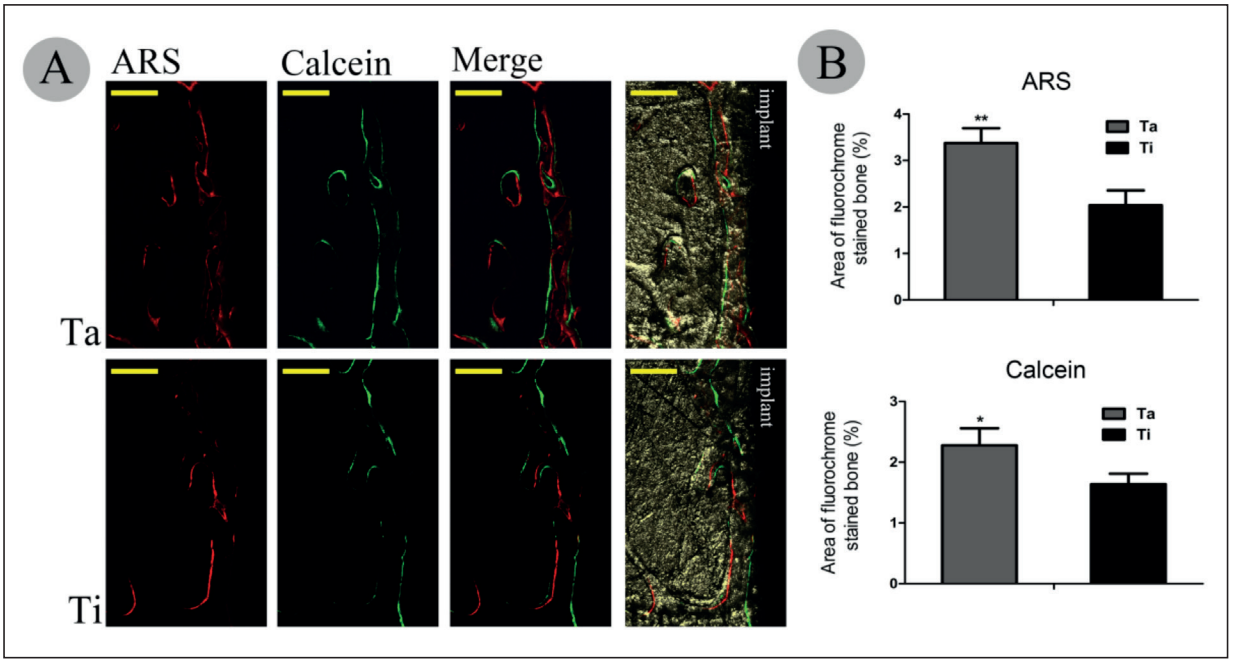

Figure 7. Histological analysis of bone formation around Ta and Ti implants in ovariectomized rats. ***A,*** Sequential fluorescent labeling of new bone on the implant surface; scale bar 200 μm. ***B,*** Area of ARS and calcein stained bone. *$p < 0.05$, **$p < 0.01$ compared with Ti.

ference regarding cell proliferation was achieved between the two substrates (Figure 1C). Such inconsistency implied that OVX-rBMSCs on the Ta surface may start to differentiate earlier at the cost of proliferation[51-53]. Furthermore, previous studies have demonstrated that the accumulation of ROS can negatively affect the viability of the surrounding cells on a Ti surface[54], with the continuous oxidative stress of such accumulation leading to the chemical degradation and physical damage of the implants[55-57]. Therefore, the lower ROS level on the Ta substrates suggested that a more favorable biological environment could be acquired around the Ta surface.

To comprehensively test the osteoinductive performance of the substrates, both CM and OM were used in our work. The results showed that the OVX-rBMSCs on the Ta substrates exhibited the highest level of ALP expression and activity (Figure 3A, B; Figure 4D, G, K; Figure S2A, E, F, J) as well as the highest degree of ECM calcification at all time points (Figure 3C, D). As ALP and calcium nodule formation function as key indicators in early and late stages of osteoblastic differentiation, respectively[58-60], the above observations clearly showed that the promoting effect of the Ta surface on OVX-rBMSC osteogenesis was continuous and could last over time. Moreover, the ALP activity on the Ti surface was elevated in comparison to that on the Cp surface in both media at day 7 (Figure 3A, B), whereas no evident difference was achieved in terms of ECM calcification (Figure 3C, D). Such findings indicated that although the Ti surface may improve OVX-BMSC osteogenesis at an early stage, the influence is not maintained over the long-term. Conversely, cells on the Ta substrates manifested the lowest expression of RANKL and the highest expression of OPG at the mRNA level (Figure 4E, F). In particular, RANKL activates osteoclastogenesis by binding to the receptor activator of NF-kB (RANK)[61], whereas OPG inhibits the interaction between RANKLE and RANK[62]. The reduced RANKL/OPG ratio resulted in the Ta surface demonstrating less favorable osteoclastogenesis as compared to that of the Ti surface. Considering that the apparent enhancement of osteoclast activity constitutes a pivotal pathological cause of osteoporosis[63], Ta might thus represent a more reasonable option as an implant surface material for use in an osteoporotic environment.

Several studies have demonstrated the promoting effect of BMP2 on BMSC osteogenesis at the cell-material interface[64,65], with BMP2 linked to the implant surface able to improve the rate of bone healing compared with that of untreated implants[66]. Furthermore, in the canonical BMP2/Smads pathway, BMP2 induces the phosphorylation of Smad1/5/8 (B-Smads); such p-B-Smads accumulate in the nucleus and regulate the transcription of genes required for osteoblastogenesis[32]. In the present work, cells on the Ta substrates exhibited evident elevation of BMP2, Smad1, RUNX2, and ALP expression at both gene and protein levels as well as Smad1 phosphorylation at all time points (Figure 5A-D, G-K; Figure S2), demonstrating that the Ta surface improved OVX-rBMSC osteogenesis by more sufficiently and continuously triggering BMP2/Smad1 signaling. Additionally, BMP2 inhibition or down-regulation of Smad1 notably reduced the elevated expression of RUNX2 and ALP on the Ta substrates (Figure 5B, D, E, G, I; Figure S4A, C, E), validating the importance of the BMP2/Smad1 cascade in mediating the effects of the Ta surface on OVX-rBMSC osteogenesis. Conversely, cells on the Ti surface overexpressing BMP2 exhibited significantly enhanced Smad1 phosphorylation and osteoblastic differentiation, indicating that the lower level of osteogenesis on the Ti surface might be associated with the insufficient activation of BMP2/Smad1 signaling. Moreover, the subsequent Smad1 interference abrogated the improvement induced by the up-regulation of BMP2 (Figure 5A-I; Figure S4), revealing the key role of Smad1 in BMP2 regulated osteogenesis. The variation of OVX-rBMSC osteogenesis consequent to the up- and down-regulation of the BMP2/Smad1 cascade on the two substrates was further confirmed by the corresponding ALP activity (Figure 5J). In addition, as BMP2 protein itself stimulates BMP2 expression[67], it is possible that the osteoinductive effect of the Ta surface was amplified by BMP2 auto-induction, which further enhanced the osteoinductivity of the material. Thus, these findings might inspire new ideas regarding the future application of Ta for subjects with osteoporosis, especially in the field of bone tissue engineering. However, several other pathways are also involved in the mediatory function of BMP2 via cross-talk, such as the non-canonical mitogen-activated protein kinase (MAPK) and phosphatidyl inositol-3-kinase/protein kinase B (PI-3K-Akt) pathways[32,68,69], as well as integrin-mediated pathways[70]. Therefore, further studies are needed to clarify the contribution of enhanced BMP2 expression with regard to the osteoinductive effect of Ta on osteoporotic cells.

The *in vivo* results of sequential fluorochrome labeling exhibited a higher grade of new bone formation and mineralization around the Ta implant at postoperative day 20 and 40 (Figure 7A, B), implying that new bone tissues formed more energetically around the Ta surface in an osteoporotic environment. Specifically, the increased incorporation of calcein into the bone along the Ta surface further validated the better osteoinductivity of Ta. Also, the larger area of ARS as compared to calcein staining in the Ta group (about 1.5:1) (Figure 7B) indicated that the Ta surface facilitated a greater degree of bone formation at an early period. These observations were in agreement with the more desirable biocompatibility and osteoinductive effect of the Ta substrates toward OVX-rBMSCs as evidenced in the present report. Although histological staining by van Gieson's picrofuchsin also showed increased bone tissue around the Ta implants, connective tissues clearly grew into the spaces between bone and both implants (Figure 6E), and the Ta implants exhibited only slightly higher BIC rates (31.82 ± 4.07% *vs.* 25.2 ± 3.84% at 8 weeks after implantation, $p = 0.052$) (Figure 6D). Such results are consistent with the report of Matsuno et al[71] using normal rats, in which Ta and Ti samples showed similar BIC despite a larger amount of newly formed bone around Ta. We consider that the low roughness of the polished surfaces may serve as the primary cause for such phenomena[72-74]. Unlike rough surfaces, polished surfaces favor the attachment of fibroblasts rather than osteoblasts[75] and are more conducive to fibrogenesis and osteoclastogenesis but inhibit angiogenesis[76-78], which greatly influences bone formation and osseointegration[79]. Moreover, the levels of integrin subunits required for enhanced osteoblast maturation are decreased on polished compared to rough surfaces[80]. Therefore, the inadequate adhesion of bone forming cells combined with their decreased osteogenic capacity in osteoporosis may have overshadowed the intrinsic osteoinductive effect of Ta *in vivo*. Considering that the use of Ta with a highly smooth surface did not guarantee enough implant osseointegration, this observation also verifies the necessity of rough and structured (nano- and micro-structured) surfaces to improve the degree of bone healing around the implants, as shown by other studies. However, roughened surfaces are also associated with inadequate epithelial cell adhesion and increased bacterial accumulation in dental implants, which may increase the chances of infection, with subsequent risk of implant failure[81]. Therefore, the most effective use of the advantages of Ta to develop implant material featuring desirable osteoinductivity *in vivo*, especially under an osteoporotic condition, remains to be ascertained.

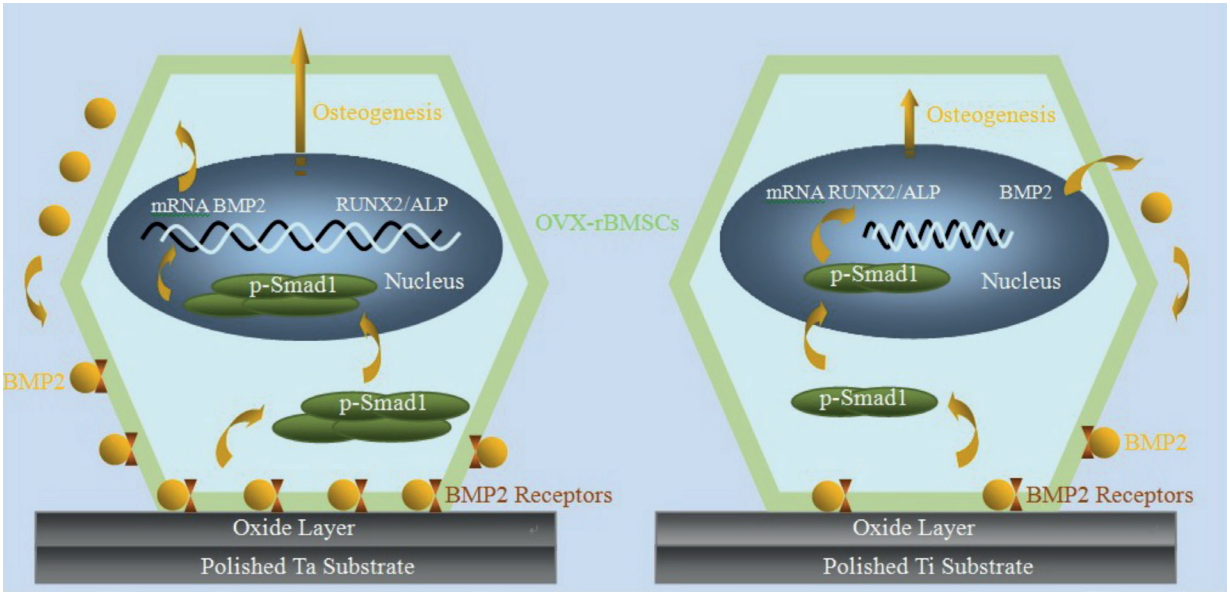

Figure 8. Possible mechanism of the osteoinductive effect exerted by Ta and Ti surfaces on OVX-rBMSCs through the BMP2/Smad-1 cascade.

Conclusions

In comparison to that of Ti, the intrinsic property of the Ta surface affords greater desirable biocompatibility toward OVX-rBMSCs and improves cell osteogenesis by more sufficiently activating BMP2/Smad1 signaling. Moreover, the Ta surface may be conducive to new bone formation under an osteoporotic condition *in vivo* (Figure 8). We suggest that Ta is superior to Ti as a surface material for the application of bone implants in osteoporosis.

Acknowledgements

This work was jointly supported by the National Natural Science Foundation of China (31370962, 31670980, 31400825, 81470714,81870806 and 81800935), Shanghai Rising-Star Program (15QA1404100), Shanghai Committee of Science and Tech-nology (15410722600 and 17441904000), Youth Innovation Promotion Association CAS (2015204), Innovation Fund of Translational Medicine of the Medical School of Shanghai Jiaotong University (15ZH2012), the Shanghai Pujiang Program (17PJD030), and Collaborative Research Program of Collaborative Innovation Center in Translational Medicine (TM201819).

Conflict of Interest

The Authors declare that they have no conflict of interests.

References

1) Cheng M, Qiao Y, Wang Q, Jin G, Qin H, Zhao Y, Peng X, Zhang X, Liu X. Calcium plasma implanted titanium surface with hierarchical microstructure for improving the bone formation. ACS Appl Mater Interfaces 2015; 7: 13053-13061.
2) Geetha M, Singh AK, Asokamani R, Gogia AK. Ti based biomaterials, the ultimate choice for orthopaedic implants – a review. Prog Mater Sci 2009; 54: 397-425.
3) Alsaadi G, Quirynen M, Komárek A, van Steenberghe D. Impact of local and systemic factors on the incidence of oral implant failures, up to abutment connection. J Clin Periodontol 2007; 34: 610-617.
4) Giro G, Chambrone L, Goldstein A, Rodrigues JA, Zenóbio E, Feres M, Figueiredo LC, Cassoni A, Shibil JA. Impact of osteoporosis in dental implants: a systematic review. World J Orthop 2015; 6: 311-315.
5) Goldhahn J, Suhm N, Goldhahn S, Blauth M, Hanson B. Influence of osteoporosis on fracture fixation--a systematic literature review. Osteoporos Int 2008; 19: 761-772.
6) Moy PK, Medina D, Shetty V, Aghaloo TL. Dental implant failure rates and associated risk factors. Int J Oral Maxillofac Implants 2005; 20: 569-577.
7) Rachner TD, Khosla S, Hofbauer LC. Osteoporosis: now and the future. Lancet 2011; 377: 1276-1287.
8) Russell LA. Osteoporosis and orthopedic surgery: effect of bone health on total joint arthroplasty outcome. Curr Rheumatol Rep 2013; 15: 371-376.
9) Cohen R. A porous tantalum trabecular metal: basic science. Am J Orthoped (Belle Mead NJ) 2002; 31: 216-217.
10) Levine BR, Sporer S, Poggie RA, Della Valle CJ, Jacobs JJ. Experimental and clinical performance of porous tantalum in orthopedic surgery. Biomaterials 2006; 27: 4671-4681.
11) Findlay DM, Welldon K, Atkins GJ, Howie DW, Zannettino AC, Bobyn D. The proliferation and phenotypic expression of human osteoblasts on tantalum metal. Biomaterials 2004; 25: 2215-2227.
12) Frandsen CJ, Brammer KS, Noh K, Johnston G, Jin S. Tantalum coating on TiO2 nanotubes induces superior rate of matrix mineralization and osteofunctionality in human osteoblasts. Mater Sci Eng C Mater Biol Appl 2014; 37: 332-341.
13) Sagomonyants KB, Hakim-Zargar M, Jhaveri A, Aronow MS, Gronowicz G. Porous tantalum stimulates the proliferation and osteogenesis of osteoblasts from elderly female patients. J Orthop Res 2011; 29: 609-616.
14) Stiehler M, Lind M, Mygind T, Baatrup A, Dolatshahi-Pirouz A, Li H, Foss M, Besenbacher F, Kassem M, Bünger C. Morphology, proliferation, and osteogenic differentiation of mesenchymal stem cells cultured on titanium, tantalum, and chromium surfaces. J Biomed Mater Res A 2008; 86: 448-458.
15) Tang Z, Xie Y, Yang F, Huang Y, Wang C, Dai K, Zheng X, Zhang X. Porous tantalum coatings prepared by vacuum plasma spraying enhance BMSCs osteogenic differentiation and bone regeneration in vitro and in vivo. PLoS One 2013; 8: e66263.
16) Di Cio S, Gautrot JE. Cell sensing of physical properties at the nanoscale: mechanisms and control of cell adhesion and phenotype. Acta Biomater 2016; 30: 26-48.
17) Huri PY, Ozilgen BA, Hutton DL, Grayson WL. Scaffold pore size modulates in vitro osteogenesis of human adipose-derived stem/stromal cells. Biomed Mater 2014; 9: 045003.
18) Rosa AL, Beloti MM. Rat bone marrow cell response to titanium and titanium alloy with different surface roughness. Clin Oral Implants Res 2003; 14: 43-48.
19) Habibovic P, de Groot K. Osteoinductive biomaterials--properties and relevance in bone repair. J Tissue Eng Regen Med 2007; 1: 25-32.
20) Olivares-Navarrete R, Hyzy SL, Hutton DL, Erdman CP, Wieland M, Boyan BD, Schwartz Z. Direct and indirect effects of microstructured titanium substrates on the induction of mesenchymal stem cell differentiation towards the osteoblast lineage. Biomaterials 2010; 31: 2728-2735.
21) Bächle M, Kohal RJ. A systematic review of the influence of different titanium surfaces on proliferation, differentiation and protein synthesis of osteoblast-like MG63 cells. Clin Oral Implants Res 2004; 15: 683-692.

22) Mustafa K, Wennerberg A, Wroblewski J, Hultenby K, Lopez BS, Arvidson K. Determining optimal surface roughness of TiO(2) blasted titanium implant material for attachment, proliferation and differentiation of cells derived from human mandibular alveolar bone. Clin Oral Implants Res 2001; 12: 515-525.

23) Rosa AL, Beloti MM. Effect of cpTi surface roughness on human bone marrow cell attachment, proliferation, and differentiation. Braz Dent J 2003; 14: 16-21.

24) Ying XZ, Qian JJ, Peng L, Zheng Q, Zhu B, Jin YH. Model research on repairing meniscus injury in rabbits using bone marrow mesenchymal stem cells and silk fibroin meniscus porous scaffold. Eur Rev Med Pharmacol Sci 2018; 22: 3689-3693.

25) Li C, Wei GJ, Xu L, Rong JS, Tao SQ, Wang YS. The involvement of senescence induced by the telomere shortness in the decline of osteogenic differentiation in BMSCs. Eur Rev Med Pharmacol Sci. 2017; 21: 1117-1124.

26) Lu T, Wen J, Qian S, Cao H, Ning C, Pan X, Jiang X, Liu X, Chu PK. Enhanced osteointegration on tantalum-implanted polyetheretherketone surface with bone-like elastic modulus. Biomaterials 2015; 51: 173-183.

27) Oreffo RO, Triffitt JT. Future potentials for using osteogenic stem cells and biomaterials in orthopedics. Bone 1999; 25: 5S-9S.

28) Zhao Y, Cao H, Qin H, Cheng T, Qian S, Cheng M, Peng X, Wang J, Zhang Y, Jin G, Zhang X, Liu X, Chu PK. Balancing the osteogenic and antibacterial properties of titanium by codoping of Mg and Ag: an in vitro and in vivo study. ACS Appl Mater Interfaces 2015; 7: 17826-17836.

29) Boeloni JN, de M Ocarino N, Silva JF, CorrÐa CR, Bertollo CM, Hell RC, de M Pereira M, Goes AM, Serakides R. Osteogenic differentiation of bone marrow mesenchymal stem cells of ovariectomized and non-ovariectomized female rats with thyroid dysfunction. Pathol Res Pract 2013; 209: 44-51.

30) Boeloni JN, Ocarino NM, Goes AM, Serakides R. Comparative study of osteogenic differentiation potential of mesenchymal stem cells derived from bone marrow and adipose tissue of osteoporotic female rats. Connect Tissue Res 2014; 55: 103-114.

31) Wang Q, Zhao B, Li C, Rong JS, Tao SQ, Tao TZ. Decreased proliferation ability and differentiation potential of mesenchymal stem cells of osteoporosis rat. Asian Pac J Trop Med 2014; 7: 358-363.

32) Chau JF, Leong WF, Li B. Signaling pathways governing osteoblast proliferation, differentiation and function. Histol Histopathol 2009; 24: 1593-1606.

33) Li B, Tian XB, Hu RY, Xu FB, Zhao JM. Mechanism of BMP and TG2 in mesenchymal stem cell osteogenesis. Eur Rev Med Pharmacol Sci 2015; 19: 4214-4219.

34) Langenfeld EM, Kong Y, Langenfeld J. Bone morphogenetic protein 2 stimulation of tumor growth involves the activation of Smad-1/5. Oncogene 2006; 25: 685-692.

35) Donoso O, Pino AM, Seitz G, Osses N, Rodriguez JP. Osteoporosis-associated alteration in the signalling status of BMP-2 in human MSCs under adipogenic conditions. J Cell Biochem 2015; 116: 1267-1277.

36) Huang B, Guang M, Ye J, Gong P, Tang H. Effect of increasing doses of gamma-radiation on bone marrow stromal cells grown on smooth and rough titanium surfaces. Stem Cells Int 2015; 2015: 359416.

37) Ozdemir T, Higgins AM, Brown JL. Osteoinductive biomaterial geometries for bone regenerative engineering. Curr Pharm Des 2013; 19:3446-3455.

38) Gao AG, Zhou YC, Hu ZJ, Lu BB. Ipriflavone promotes osteogenesis of MSCs derived from osteoporotic rats. Eur Rev Med Pharmacol Sci 2018; 22: 4669-4676.

39) Xia L, Yin Z, Mao L, Wang X, Liu J, Jiang X, Lin K, Chang J, Fang B. Akermanite bioceramics promote osteogenesis, angiogenesis and suppress osteoclastogenesis for osteoporotic bone regeneration. Sci Rep 2016; 6: 22005.

40) Turner AS. Animal models of osteoporosis--necessity and limitations. Eur Cell Mater 2001; 1: 66-81.

41) Javed F, Vohra F, Zafar S, Almas K. Significance of osteogenic surface coatings on implants to enhance osseointegration under osteoporotic-like conditions. Implant Dent 2014; 23: 679-686.

42) Oue H, Doi K, Oki Y, Makihara Y, Kubo T, Perrotti V, Piattelli A, Akagawa Y, Tsuga K. Influence of implant surface topography on primary stability in a standardized osteoporosis rabbit model study. J Funct Biomater 2015; 6: 143-152.

43) Xin Y, Jiang J, Huo K, Hu T, Chu PK. Bioactive Sr-TiO(3) nanotube arrays: strontium delivery platform on Ti-based osteoporotic bone implants. ACS Nano 2009; 3: 3228-3234.

44) Yang G, Song L, Guo C, Zhao S, Liu L, He F. Bone responses to simvastatin-loaded porous implant surfaces in an ovariectomized model. Int J Oral & Maxillofac Implants 2012; 27: 369-374.

45) Hoerth RM, Katunar MR, Gomez Sanchez A, Orellano JC, Ceré SM, Wagermaier W, Ballarre J. A comparative study of zirconium and titanium implants in rat: osseointegration and bone material quality. J Mater Sci Mater Med 2014; 25: 411-422.

46) Ogle OE. Implant surface material, design, and osseointegration. Dent Clin North Am 2015; 59: 505-520.

47) Bächle M, Kohal RJ. A systematic review of the influence of different titanium surfaces on proliferation, differentiation and protein synthesis of osteoblast-like MG63 cells. Clin Oral Implants Res 2004; 15: 683-692.

48) van Midwoud PM, Janse A, Merema MT, Groothuis GM, Verpoorte E. Comparison of biocompatibility and adsorption properties of different plastics for advanced microfluidic cell and tissue culture models. Anal Chem 2012; 84: 3938-3944.

49) Tasnim N, Kumar A, Joddar B. Attenuation of the in vitro neurotoxicity of 316L SS by graphene oxide surface coating. Mater Sci Eng C Mater Biol Appl 2017; 73: 788-797.

50) Mouthuy PA, Snelling SJB, Dakin SG, Milković L, Gašparović AČ, Carr AJ, Žarković N. Biocompatibility of implantable materials: An oxidative stress viewpoint. Biomaterials 2016; 109: 55-68.

51) Boyan BD, Lossdörfer S, Wang L, Zhao G, Lohmann CH, Cochran DL, Schwartz Z. Osteoblasts generate an osteogenic microenvironment when grown on surfaces with rough microtopographies. Eur Cell Mater 2003; 6: 22-27.

52) Lohmann CH, Bonewald LF, Sisk MA, Sylvia VL, Cochran DL, Dean DD, Boyan BD, Schwartz z. Maturation state determines the response of osteogenic cells to surface roughness and 1,25-dihydroxyvitamin D3. J Bone Miner Res 2000; 15: 1169-1180.

53) Zhao L, Mei S, Chu PK, Zhang Y, Wu Z. The influence of hierarchical hybrid micro/nano-textured titanium surface with titania nanotubes on osteoblast functions. Biomaterials 2010; 31: 5072-5082.

54) Lee YH, Lee NH, Bhattarai G, Oh YT, Yu MK, Yoo ID, Jhee EC, Yi HK. Enhancement of osteoblast biocompatibility on titanium surface with Terrein treatment. Cell Biochem Funct 2010; 28: 678-685.

55) Anderson JM, Rodriguez A, Chang DT. Foreign body reaction to biomaterials. Semin Immunol 2008; 20: 86-100.

56) Christo SN, Diener KR, Bachhuka A, Vasilev K, Hayball JD. Innate immunity and biomaterials at the nexus: friends or foes. Biomed Res Int 2015; 2015: 342304.

57) Luttikhuizen DT, Harmsen MC, Van Luyn MJ. Cellular and molecular dynamics in the foreign body reaction. Tissue Eng 2006; 12: 1955-1970.

58) Liu H, Wei LK, Jian XF, Huang J, Zou H, Zhang SZ, Yuan GH. Isolation, culture and induced differentiation of rabbit mesenchymal stem cells into osteoblasts. Exp Ther Med 2018; 15: 3715-3724.

59) Elashry MI, Baulig N, Heimann M, Bernhardt C, Wenisch S, Arnhold S. Osteogenic differentiation of equine adipose tissue derived mesenchymal stem cells using CaCl2. Res Vet Sci 2018; 117: 45-53.

60) Whyte MP. Hypophosphatasia and the role of alkaline phosphatase in skeletal mineralization. Endocr Rev 1994; 15: 439-461.

61) Yamaguchi Y, Sakai E, Sakamoto H, Fumimoto R, Fukuma Y, Nishishita K, Okamoto K, Tsukuba T. Inhibitory effects of tert-butylhydroquinone on osteoclast differentiation via up-regulation of heme oxygenase-1 and down-regulation of HMGB1 release and NFATc1 expression. J Appl Toxicol 2014; 34: 49-56.

62) Park K, Ju WC, Yeo JH, Kim JY, Seo HS, Uchida Y, Cho Y. Increased OPG/RANKL ratio in the conditioned medium of soybean-treated osteoblasts suppresses RANKL-induced osteoclast differentiation. Int J Mol Med 2014; 33: 178-184.

63) Tella SH, Gallagher JC. Prevention and treatment of postmenopausal osteoporosis. J Steroid Biochem Mol Biol 2014; 142: 155-170.

64) Han L, Lin H, Lu X, Zhi W, Wang KF, Meng FZ, Jiang O. BMP2-encapsulated chitosan coatings on functionalized Ti surfaces and their performance in vitro and in vivo. Mater Sci Eng C Mater Biol Appl 2014; 40: 1-8.

65) Shah NJ, Hyder MN, Moskowitz JS, Quadir MA, Morton SW, Seeherman HJ, Padera RF, Spector M, Hammond PT. Surface-mediated bone tissue morphogenesis from tunable nanolayered implant coatings. Sci Transl Med 2013; 5: 191ra83.

66) Seol YJ, Park YJ, Lee SC, Kim KH, Lee JY, Kim TI, Lee YM, Ku Y, Rhyu IC, Han SB, Chung CP. Enhanced osteogenic promotion around dental implants with synthetic binding motif mimicking bone morphogenetic protein (BMP)-2. J Biomed Mater Res A 2006; 77: 599-607.

67) Ghosh-Choudhury N, Choudhury GG, Harris MA, Wozney J, Mundy GR, Abboud SL, Harris SE. Autoregulation of mouse BMP-2 gene transcription is directed by the proximal promoter element. Biochem Biophys Res Commun 2001; 286: 101-108.

68) Miyazono K, Maeda S, Imamura T. BMP receptor signaling: transcriptional targets, regulation of signals, and signaling cross-talk. Cytokine Growth Factor Rev 2005; 16: 251-263.

69) Osyczka AM, Leboy PS. Bone morphogenetic protein regulation of early osteoblast genes in human marrow stromal cells is mediated by extracellular signal-regulated kinase and phosphatidylinositol 3-kinase signaling. Endocrinology 2005; 146: 3428-3437.

70) Marie PJ. Targeting integrins to promote bone formation and repair. Nat Rev Endocrinol 2013; 9: 288-295.

71) Matsuno H, Yokoyama A, Watari F, Uo M, Kawasaki T. Biocompatibility and osteogenesis of refractory metal implants, titanium, hafnium, niobium, tantalum and rhenium. Biomaterials 2001; 22: 1253-1262.

72) Hara T, Matsuoka K, Matsuzaka K, Yoshinari M, Inoue T. Effect of surface roughness of titanium dental implant placed under periosteum on gene expression of bone morphogenic markers in rat. Bull Tokyo Dent Coll 2012; 53: 45-50.

73) Hoffmann O, Angelov N, Zafiropoulos GG, Andreana S. Osseointegration of zirconia implants with different surface characteristics: an evaluation in rabbits. Int J Oral Maxillofac Implants 2012; 27: 35235-35238.

74) Ravichandran R, Ng C, Liao S, Pliszka D, Raghunath M, Ramakrishna S, Chan CK. Biomimetic surface modification of titanium surfaces for early cell capture by advanced electrospinning. Biomed Mater 2012; 7: 015001.

75) Schuler M, Owen GR, Hamilton DW, de Wild M, Textor M, Brunette DM, Tosatti SG. Biomimet-

ic modification of titanium dental implant model surfaces using the RGDSP-peptide sequence: a cell morphology study. Biomaterials 2006; 27: 4003-4015.

76) Mendonca DB, Miguez PA, Mendonca G, Yamauchi M, Aragao FJ, Cooper LF. Titanium surface topography affects collagen biosynthesis of adherent cells. Bone 2011; 49: 463-472.

77) Olivares-Navarrete R, Hyzy SL, Slosar PJ, Schneider JM, Schwartz Z, Boyan BD. Implant materials generate different peri-implant inflammatory factors: poly-ether-ether-ketone promotes fibrosis and microtextured titanium promotes osteogenic factors. Spine (Phila Pa 1976) 2015; 40: 399-404.

78) Olivares-Navarrete R, Hyzy SL, Gittens RA 1st, Schneider JM, Haithcock DA, Ullrich PF, Slosar PJ, Schwartz Z, Boyan BD. Rough titanium alloys regulate osteoblast production of angiogenic factors. Spine J 2013; 13: 1563-1570.

79) Abshagen K, Schrodi I, Gerber T, Vollmar B. In vivo analysis of biocompatibility and vascularization of the synthetic bone grafting substitute NanoBone. J Biomed Mater Res A 2009; 91: 557-566.

80) Olivares-Navarrete R, Raz P, Zhao G, Chen J, Wieland M, Cochran DL, Chaudhri RA, Omoy A, Boyan BD, Schwartz Z. Integrin alpha2beta1 plays a critical role in osteoblast response to micron-scale surface structure and surface energy of titanium substrates. Proc Natl Acad Sci U S A 2008; 105: 15767-15772.

81) Bürgers R, Gerlach T, Hahnel S, Schwarz F, Handel G, Gosau M. In vivo and in vitro biofilm formation on two different titanium implant surfaces. Clin Oral Implants Res 2010; 21: 156-164.